Supporting Information

Highly intrinsic thermal conductivity of cellulose nanocrystals films through pitch regulation

Jianyu Zhang,[a] Tianxing Chen,[a] Siyuan Liu,[a] Zhixin Chen,[b] Yao Li,[a] Shenmin Zhu,*[a] and Hua Li*[a] [a] State Key Laboratory of Metal Matrix Composites, Shanghai Jiao Tong University, Shanghai 200240, China.

[b] School of Mechanical, Materials & Mechatronics Engineering, University of Wollongong, Wollongong, NSW 2522, Australia.

* Corresponding author. E-mail: smzhu@sjtu.edu.cn

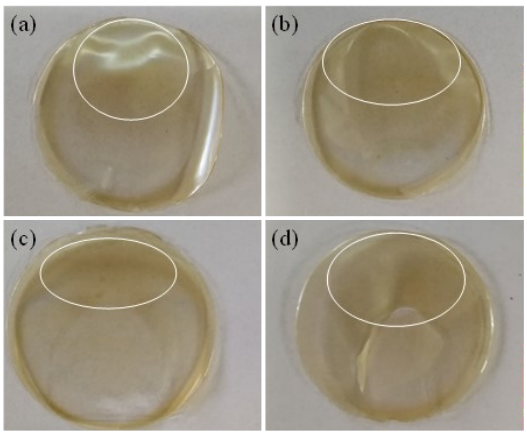

Fig. S1 Optical images of (a) CNCs- Fe_3O_4/CNC-1.10-H11-90 film, (b) CNCs- Fe_3O_4/CNC-1.10-H23-90 film, (c) CNCs- Fe_3O_4/CNC-1.10-H11-45 film, (d) CNCs- Fe_3O_4/CNC-1.10-H23-45 film. 90 and 45 represent the angle of the vertical magnetic field tilt. Fe_3O_4/CNC agglomeration appeared in all films. The white circles circled the reunion areas.

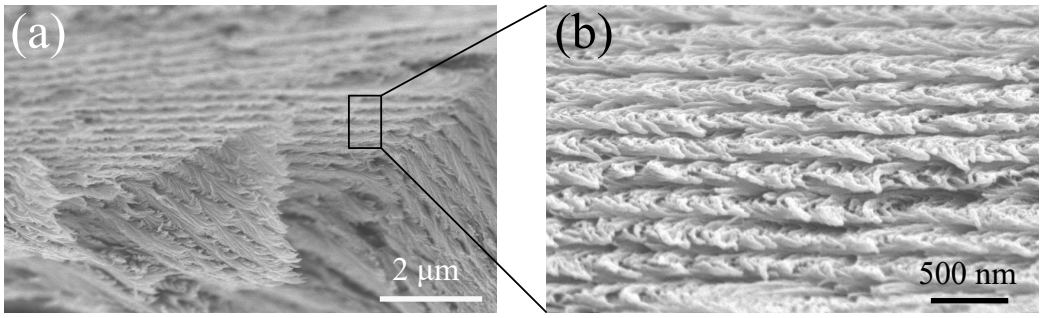

Fig. S2 SEM images of oblique section of the CNC-Fe_3O_4/CNC film, (a) and (b).in different magnifications.

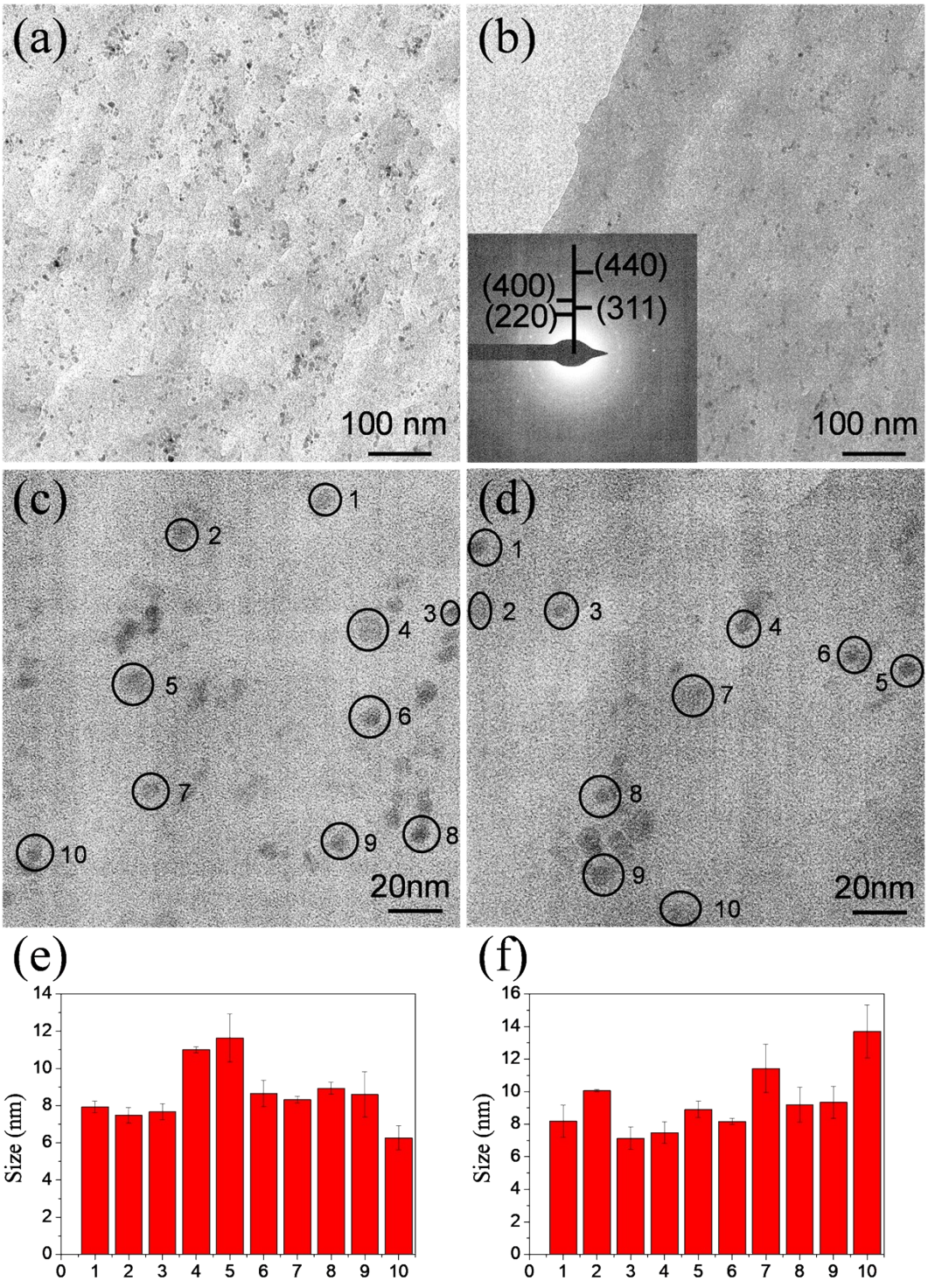

Fig. S3 The cross-section TEM images of CNC-Fe_3O_4/CNC-1.10 film (a, c, d), the selected area electron diffraction (SAED) pattern of one Fe_3O_4 particle shown in (b), measurement results of the Fe_3O_4 particle size from Fig. S3c image (e), measurement results of the Fe_3O_4 particle size from Fig. S3d image (f).

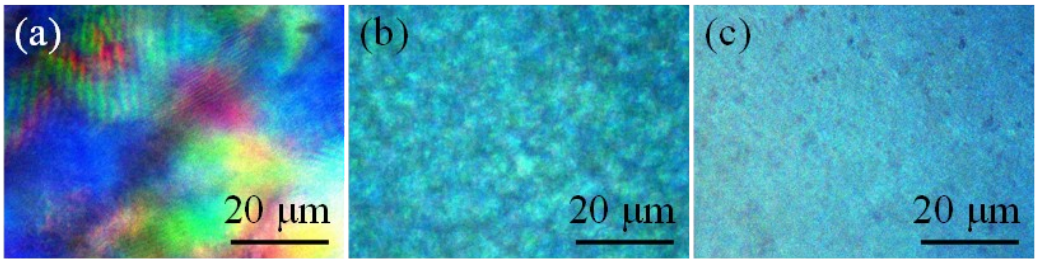

Fig. S4 POM images of (a) CNCs film, (b) CNC-Fe_3O_4/CNC-1.90 film, (c) CNC-Fe_3O_4/CNC-2.84 film.

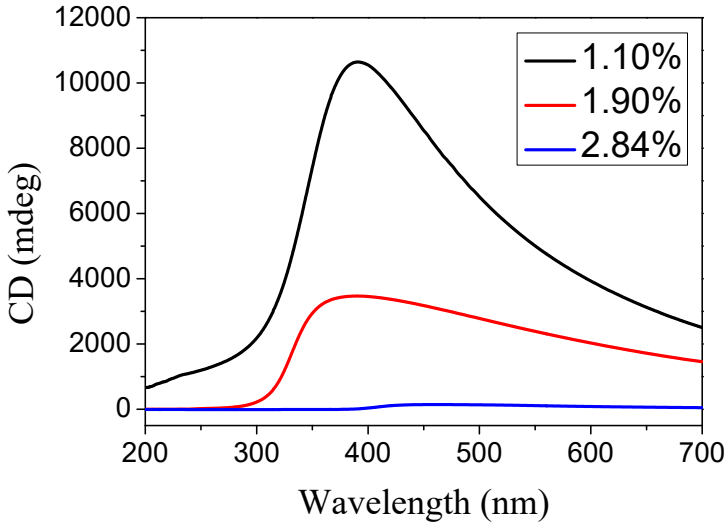

Fig. S5 Circular dichroism spectra for CNC-Fe_3O_4/CNC-1.10 film, CNC-Fe_3O_4/CNC-1.90 film, and CNC-Fe_3O_4/CNC-2.84 film.

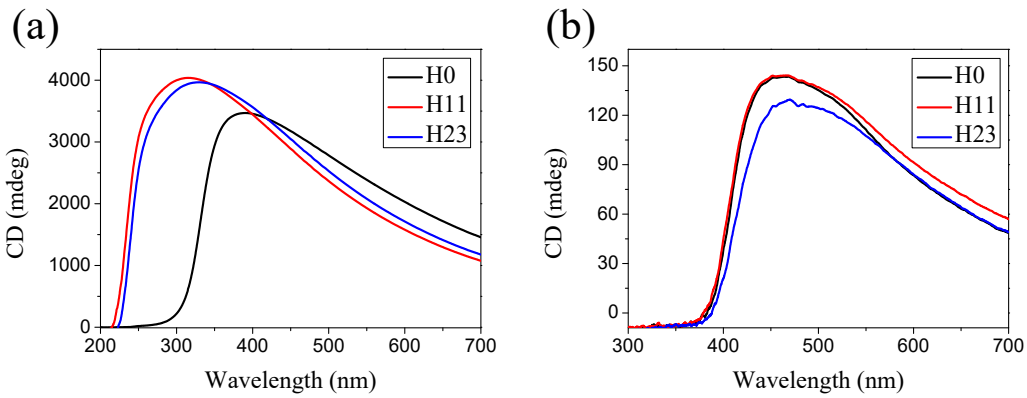

Fig. S6 Circular dichroism spectra of (a) CNC-Fe_3O_4/CNC-1.90 films, (b) CNC-Fe_3O_4/CNC-2.84 films formed under different magnetic field intensities.

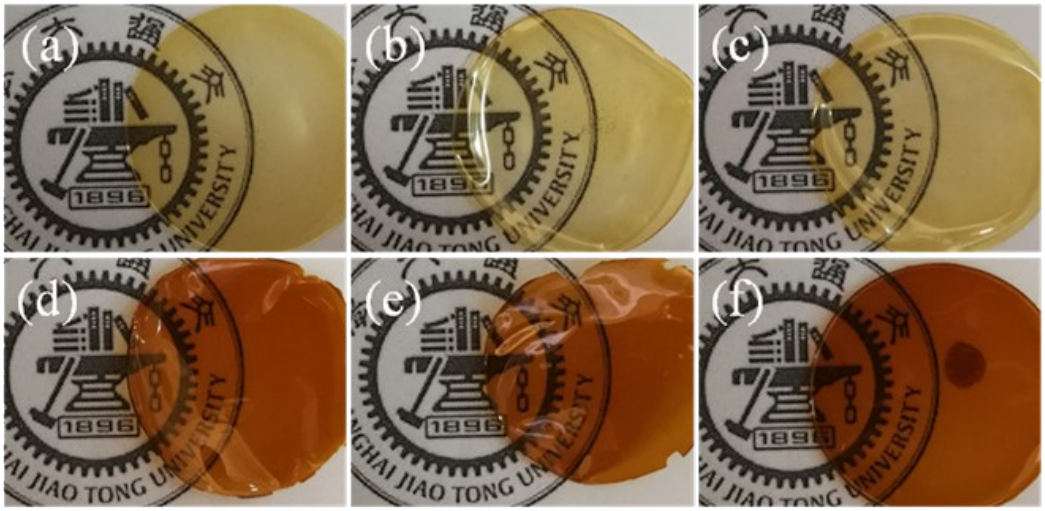

Fig. S7 Optical images of (a) CNC-Fe_3O_4/CNC-1.90-H0 film, (b) CNC-Fe_3O_4/CNC-1.90-H11 film, (c) CNC-Fe_3O_4/CNC-1.90-H23 film, (d) CNC-Fe_3O_4/CNC-2.84-H0 film, (e) CNC-Fe_3O_4/CNC-2.84-H11 film, (f) CNC-Fe_3O_4/CNC-2.84-H23 film.

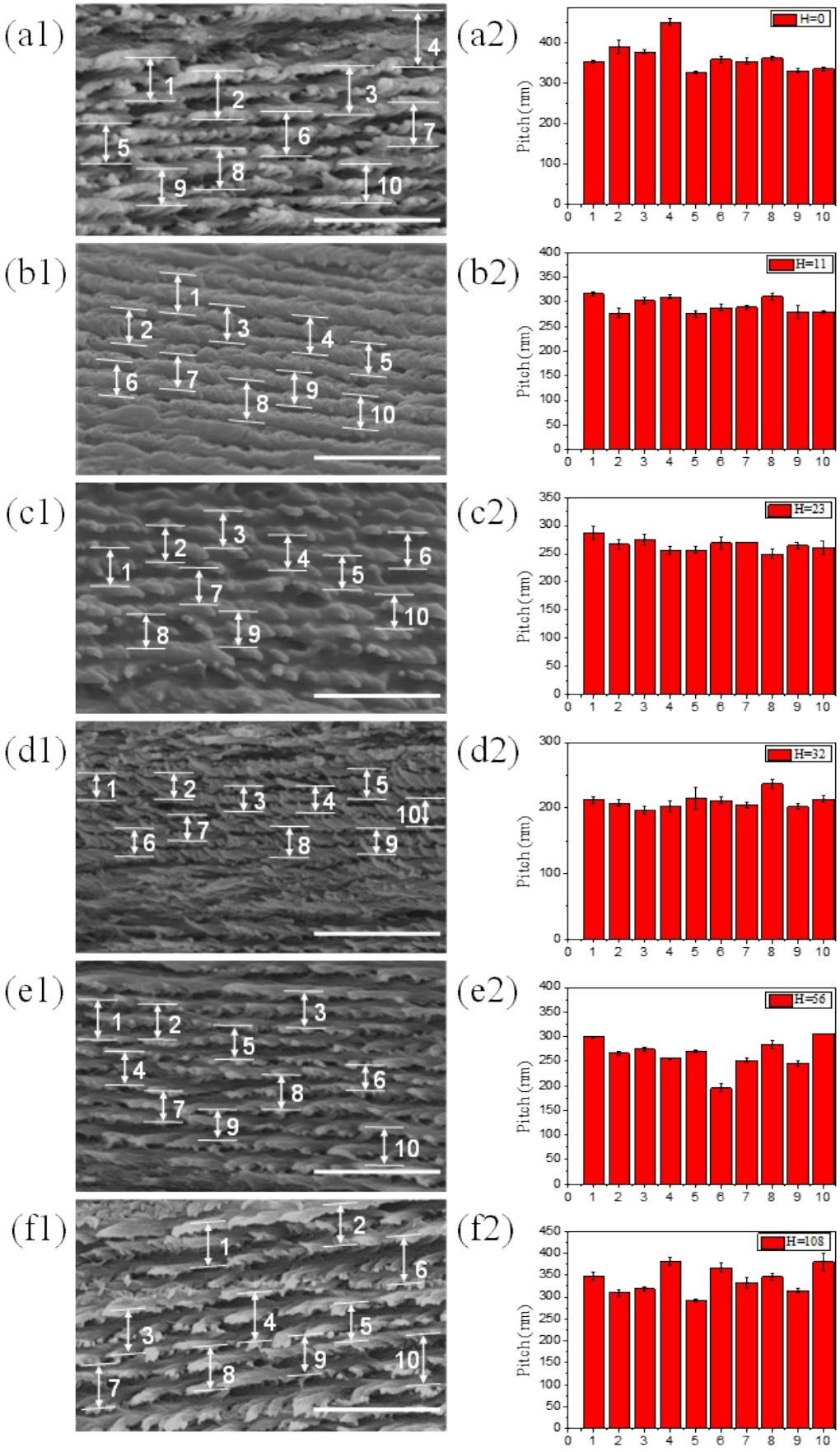
(a1)
(a2)
H=0
(b1)
(b2)
H=11
(c1)
(c2)
H=23
(d1)
(d2)
H=32
(e1)
(e2)
H=56
(f1)
(f2)
H=108
Pitch (nm)

Fig. S8 SEM images of cross-sections of the CNC-Fe_3O_4/CNC-1.10 films formed under different magnetic field intensities and the pitch sizes measured from the images. The scale bar is 1 μm. (a1) and (a2) 0 mT, (b1) and (b2) 11 mT, (c1) and (c2) 23 mT, (d1) and (d2) 32mT, (e1) and (e2) 56 mT, (f1) and (f2) 108 mT.

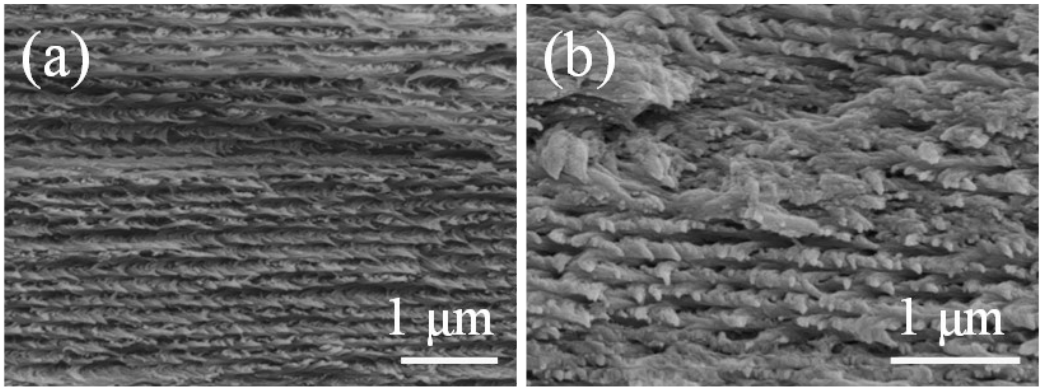

Fig. S9 SEM images of cross-sections of the CNC-Fe_3O_4/CNC-1.10 films formed under magnetic field intensity of (a) 32 mT, (b) 108 mT.

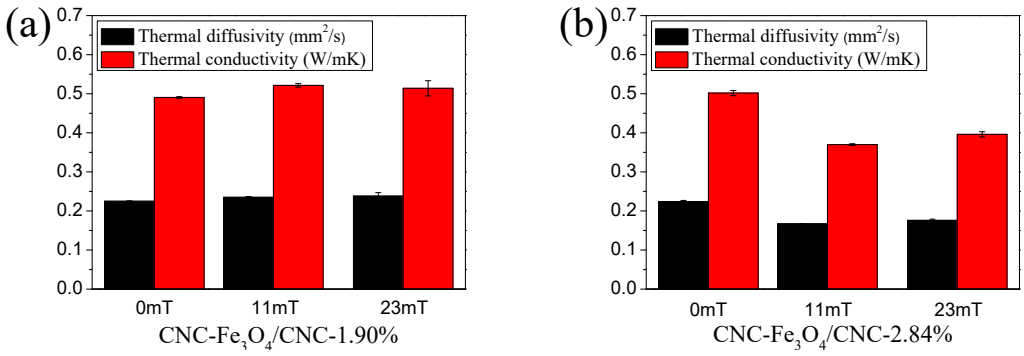

Fig. S10 The out-plane thermal diffusivities (TD) and thermal conductivities (TC) of (a) CNC-Fe_3O_4/CNC-1.90 films, (b) CNC-Fe_3O_4/CNC-2.84 films under different magnetic field intensities.

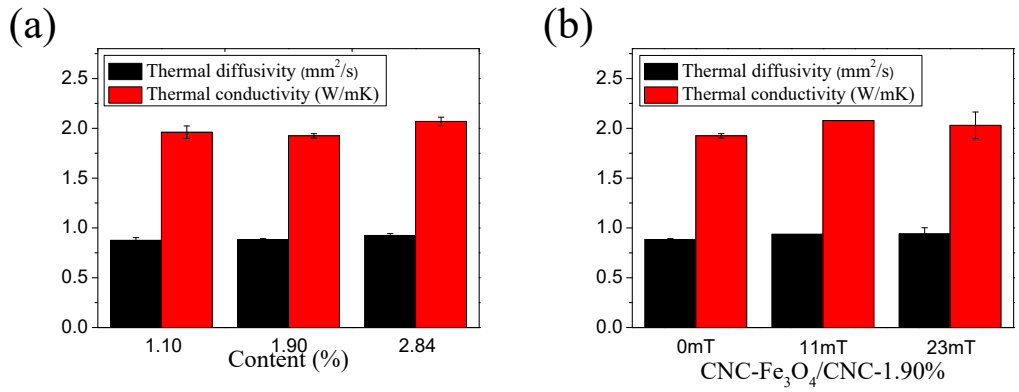

Fig. S11 The in-plane thermal diffusivities (TD) and thermal conductivities (TC) of (a) films with different contents of Fe_3O_4, (b) CNC-Fe_3O_4/CNC-1.90 films formed under different magnetic field intensities.

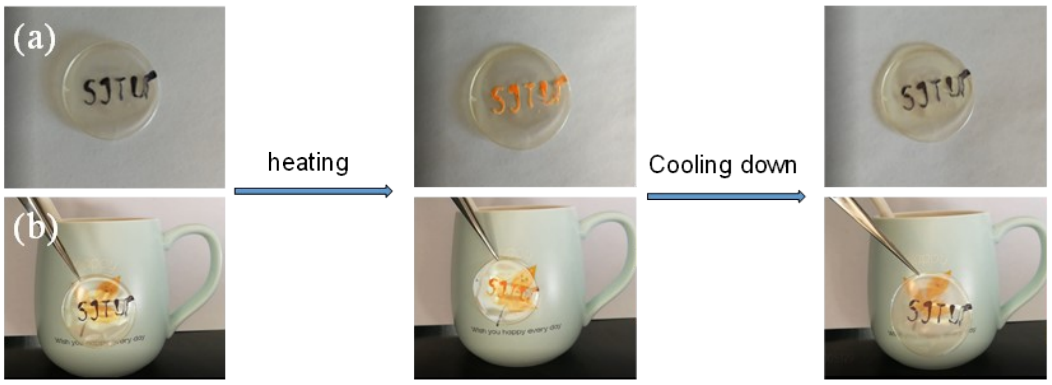

Fig. S12 The transparent CNC-Fe_3O_4/CNC-1.10-H32 film as thermochromic membrane.

The crystallinity (X_C) of CNCs can be calculated by Segal's method:

$$X_C = ((I_{002} - I_{am}) / I_{002}) \times 100$$

where I_{am} is the diffraction intensity of o the amorphous phase taken at angle around 18° - 19°. I_{002} is the intensity of the (0 0 2) peak, which is the maximum intensity in XRD. From the XRD pattern in Fig. 2b, the crystallinities of the CNCs prepared by us and CNCs in Fe_3O_4/CNC are caculated as:

Table S1 The crystallinities of CNCs and CNCs in Fe_3O_4/CNC

Sample	I_{002}	I_{am}	X_C
CNCs	1778	218	87.7 %
CNCs in Fe_3O_4/CNC	373	45	87.9 %

Table S2 Through-plane thermal conductivities

Sample	Thermal diffusivity (mm^2s^{-1})	Density ($g\ cm^{-3}$)	specific heat capacity ($J\ g^{-1}\ k^{-1}$)	Thermal conductivity ($Wm^{-1}K^{-1}$)
CNCs	0.197±0.002	1.479	1.539	0.448±0.005
CNC-Fe_3O_4/CNC-1.10-H0	0.211±0.003	1.504	1.490	0.473±0.007
CNC-Fe_3O_4/CNC-1.10-H11	0.237±0.005	1.523		0.538±0.011
CNC-Fe_3O_4/CNC-1.10-H23	0.263±0.003	1.532		0.600±0.007
CNC-Fe_3O_4/CNC-1.10-H32	0.351±0.003	1.525		0.798±0.007
CNC-Fe_3O_4/CNC-1.10-H56	0.349±0.003	1.518		0.790±0.007
CNC-Fe_3O_4/CNC-1.10-H108	0.309±0.005	1.518		0.699±0.011
CNC-Fe_3O_4/CNC-1.90-H0	0.225±0.001	1.496	1.457	0.490±0.002
CNC-Fe_3O_4/CNC-1.90-H11	0.235±0.002	1.523		0.521±0.004
CNC-Fe_3O_4/CNC-1.90-H23	0.238±0.009	1.482		0.514±0.019
CNC-Fe_3O_4/CNC-2.84-H0	0.224±0.003	1.518	1.475	0.502±0.007
CNC-Fe_3O_4/CNC-2.84-H11	0.167±0.001	1.501		0.370±0.002
CNC-Fe_3O_4/CNC-2.84-H23	0.176±0.003	1.525		0.396±0.007

Table S3 In-plane thermal conductivities

Sample	Thermal diffusivity (mm^2s^{-1})	Density ($g\ cm^{-3}$)	specific heat capacity ($J\ g^{-1}\ k^{-1}$)	Thermal conductivity ($Wm^{-1}K^{-1}$)
CNC-Fe_3O_4/CNC-1.10-H0	0.875±0.028	1.504	1.490	1.961±0.063
CNC-Fe_3O_4/CNC-1.90-H0	0.883±0.01	1.496	1.457	1.925±0.022
CNC-Fe_3O_4/CNC-1.90-H11	0.936±0.00	1.523		2.077±0.00
CNC-Fe_3O_4/CNC-1.90-H23	0.94±0.062	1.482		2.030±0.134
CNC-Fe_3O_4/CNC-2.84-H0	0.924±0.019	1.518	1.475	2.069±0.043